Original Article | Neuroimaging and Head & Neck

http://dx.doi.org/10.3348/kjr.2016.17.5.657
pISSN 1229-6929 · eISSN 2005-8330
Korean J Radiol 2016;17(5):657-663

Korean Journal of Radiology
KJR

Superior Cervical Sympathetic Ganglion: Normal Imaging Appearance on 3T-MRI

Joo Yeon Lee, MD[1], Jeong Hyun Lee, MD, PhD[1], Joon Seon Song, MD[2], Min Jeong Song, MD[2], Seung-Jun Hwang, MD[3], Ra Gyoung Yoon, MD[4], Seung Won Jang, MD[1], Ji Eun Park, MD, PhD[1], Young Jin Heo, MD[5], Young Jun Choi, MD[1], Jung Hwan Baek, MD, PhD[1]

Departments of [1]Radiology and Research Institute of Radiology, [2]Pathology, and [3]Anatomy and Cell Biology, University of Ulsan College of Medicine, Asan Medical Center, Seoul 05505, Korea; [4]Department of Radiology, Catholic Kwandong University International St. Mary's Hospital, Catholic Kwandong University College of Medicine, Incheon 22711, Korea; [5]Department of Radiology, Busan Paik Hospital, Inje University College of Medicine, Busan 47392, Korea

Objective: To identify superior cervical sympathetic ganglion (SCSG) and describe their characteristic MR appearance using 3T-MRI.

Materials and Methods: In this prospective study, we recruited 53 consecutive patients without history of head and neck irradiation. Using anatomic location based on literature review, both sides of the neck were evaluated to identify SCSGs in consensus. SCSGs were divided into definite (medial to internal carotid artery [ICA] and lateral to longus capitis muscle [LCM]) and probable SCSGs based on relative location to ICA and LCM. Two readers evaluated signal characteristics including intraganglionic hypointensity of all SCSGs and relative location of probable SCSGs. Interrater and intrarater agreements were quantified using unweighted kappa.

Results: Ninety-one neck sites in 53 patients were evaluated after exclusion of 15 neck sites with pathology. Definite SCSGs were identified at 66 (73%) sites, and probable SCSGs were found in 25 (27%). Probable SCSGs were located anterior to LCM in 16 (18%), lateral to ICA in 6 (7%), and posterior to ICA in 3 (3%). Intraganglionic hypointensity was identified in 82 (90%) on contrast-enhanced fat-suppressed T1-weighted images. There was no statistical difference in the relative location between definite and probable SCSGs of the right and left sides with intragnalionic hypointensity on difference pulse sequences. Interrater and intrarater agreements on the location and intraganglionic hypointensity were excellent (κ-value, 0.749–1.000).

Conclusion: 3T-MRI identified definite SCSGs at 73% of neck sites and varied location of the remaining SCSGs. Intraganglionic hypointensity was a characteristic feature of SCSGs.

Keywords: *Magnetic resonance imaging; Cervical; Neck; Ganglia; Sympathetic; Anatomy; Variation*

Received August 3, 2015; accepted after revision June 10, 2016.
Corresponding author: Jeong Hyun Lee, MD, PhD, Department of Radiology and Research Institute of Radiology, University of Ulsan College of Medicine, Asan Medical Center, 88 Olympic-ro 43-gil, Songpa-gu, Seoul 05505, Korea.
• Tel: (822) 3010-4400 • Fax: (822) 476-0090
• E-mail: jeonghlee@amc.seoul.kr

INTRODUCTION

The superior, middle, and inferior ganglia comprise the cervical portion of the sympathetic system. As the most cranial part of the paravertebral sympathetic trunk, the superior cervical sympathetic ganglion (SCSG) is the largest of the three and serves to distribute sympathetic fibers to the head and neck region (1, 2). It is composed of multipolar ganglion cells with intervening nerve fibers, and receives two or three branches from the ascending

pharyngeal artery (3). Previous cadaveric studies described the SCSG as fusiform or flattened in shape and embedded within connective tissue anterior to the transverse process of the second, third, and rarely, the fourth cervical vertebrae (2, 4, 5). Its location has been confirmed by several reports (2, 4, 6-9).

Clinically, pathologies of the SCSG, including iatrogenic injuries during spine surgery, can result in Horner's syndrome; ipsilateral blepharoptosis, miosis, and facial anhydrosis (6, 10). For patients with neuropathic facial pain, such as trigeminal neuralgia or postherpetic neuralgia, percutaneous nerve block of the SCSGs can provide pain relief and is an alternative to stellate ganglion block (1, 11, 12). Therefore, it is important to determine the precise anatomical location of the SCSG on pre-procedural imaging.

Recently, Yuen et al. (13) reported a case of enlarged SCSG after radiation therapy for nasopharyngeal carcinoma-mimicking metastatic retropharyngeal lymph node, which presented as a well-defined mass with avid enhancement at the level of the C2 vertebra on 3T-MRI. Normal imaging appearance of SCSGs and characteristics that differentiate SCSGs from retropharyngeal lymphadenopathy remain to be determined. To the best of our knowledge, there are no reports of the normal imaging appearance of SCSG on neck MRI, including anatomical variations. We intended to assess the imaging anatomy of normal SCSGs on 3T-MRI using predefined anatomical criteria and evaluate MRI features of SCSGs to differentiate them from pathologies such as retropharyngeal lymphadenopathy. In our clinical experience, we frequently observe intraganglionic hypointensity near the center of SCSGs on axial MR images, hence, we also determined whether intraganglionic hypointensity might be a characteristic finding of SCSGs.

MATERIALS AND METHODS

Study Population

This prospective study was approved by the Institutional Review Board of our hospital, and written informed consent for MR imaging was obtained from all participants. Between January 2013 and June 2013, 119 consecutive patients underwent contrast-enhanced (CE) MR imaging of the neck for primary head and neck cancer evaluation or surveillance after excision of a benign soft tissue tumor. Sixty-six patients with history of previous neck irradiation that might affect the MR signal intensity of neural structures were excluded. Two sites in each of the remaining 53 patients were included in this study (26 men and 27 women; average age, 56 years; age range, 25–76 years).

MRI Technique

All examinations were conducted using a 3T MR unit (Achieva, Philips Medical Systems, Best, the Netherlands) and a 16-element phased array sensitivity-encoding neurovascular coil (SENSE NV coil, Philips Medical Systems, Best, the Netherlands). The neck MR imaging protocol included coronal fat-suppressed (FS) axial T2-weighted images (T2WI) and coronal T2WI, T1-weighted images (T1WI), and CE FS T1WI with 3–4 mm slice thickness without gaps. Axial T2WI were obtained with the following parameters: repetition time = 4100 ms; echo time = 100 ms; number of excitations = 2; number of phase encoding steps = 271; echo train length = 16; flip angle = 90°; field-of-view = 230 x 190 mm; acquisition matrix = 272 x 271 (reconstruction matrix = 512 x 512); section thickness = 3 mm; and spacing between sections = 3 mm. Axial T1WI were obtained with the following parameters: repetition time = 600 ms; echo time = 8.8 ms; number of excitations = 2; number of phase encoding steps = 232; echo train length = 5; flip angle = 90°; field-of-view = 230 x 190 mm; acquisition matrix = 236 x 232 (reconstruction matrix = 512 x 512); section thickness = 3 mm; and spacing between sections = 3 mm. Spectral presaturation with inversion recovery pulse was applied for all FS sequences. Gadoterate meglumine (0.1 mmol/kg body weight; Dotarem; Guerbet, Paris, France) was injected intravenously and CE FS T1WI was acquired after 3–8 minutes.

Imaging Interpretation

Two radiologists with 18 years and 3 years experience of head and neck imaging defined the anatomical criteria for SCSGs. These criteria were based on a literature search of the PubMed database with the following title search terms: superior sympathetic ganglion, cervical ganglion, sympathetic trunk, sympathetic ganglia, anatomy, or cadaveric in their title. The search revealed six cadaveric studies that described the anatomical location and shape of SCSGs (1, 4, 6, 8, 9, 14) in 10 to 52 enrolled subjects. The following four criteria were used for classification of a neck structure as the SCSG: 1) vertically-oriented fusiform or ovoid-shaped; 2) located medial to the internal carotid artery (ICA) and lateral to the longus capitis muscle (LCM); 3) at the level between the C2 and C4 vertebrae; and 4) between 13.1 and 45.7 mm in length and 3.8 and 17.6 mm

Korean Journal of Radiology
KJR

in width.

Step 1. Consensus Reading

Two head and neck radiologists used strict diagnostic criteria in consensus to identify definite SCSGs. The following characteristics were evaluated for each of the identified SCSGs: MR signal intensities, contrast enhancement pattern, and intraganglionic hypointensity. Intraganglionic hypointensity was defined as a tiny hypointense dot near the center of the SCSG that continued for more than one consecutive axial image along the longitudinal axis of the SCSG. Cases with an abnormality or any confusing structure in the retropharyngeal, parapharyngeal or prevertebral space at the level between the C2 and C4 vertebrae were excluded. Structures that met all criteria except the relative location to the ICA or the LCM and had the same MR signal characteristics were defined as probable SCSGs.

Step 2. Independent Reading

The relative location of all probable SCSGs were assessed independently by the same radiologists (Fig. 1) as medial, lateral, anterior, or posterior to the ICA and as anterior or lateral to the LCM.

For each of the definite and probable SCSGs, the presence of intraganglionic hypointensity was identified on T2WI, T1WI, and CE FS T1WI.

Interrater agreement was determined for the relative anatomical location, and the presence of intraganglionic hypointensity of definite and probable SCSGs for each pulse sequence (T2WI, T1WI, and CE FS T1WI). One of the radiologists performed the same analysis after a 3 week interval to determine intrarater agreement.

The level of the SCSG relative to the cervical spine was determined and the three-dimensional size of the SCSG was measured using a tool equipped with a picture archiving and communication system workstation.

Step 3. Additional Ex Vivo and In Vivo Examinations

Two pathologists performed a histologic examination of the ganglia harvested from an adult cadaver donated to University of Ulsan College of Medicine. Two radiologists and two pathologists correlated the intraganglionic hypointensity seen on 3T-MRI with the microscopic findings of the SCSG. Moreover, susceptibility weighted imaging, in addition to the aforementioned sequences of conventional 3T-MRI, was performed on a 59-year-old male participant with the following parameters: repetition time = 26 ms; echo time = 20 ms; flip angle = 17°; bandwidth = 240 Hz/pixel; spatial resolution = 0.48 x 0.48 x 2.0 mm^3; acquisition matrix = 448 x 314 (reconstruction matrix = 216 x 264); and field-of-view = 210 mm.

Statistical Analysis

Statistical analysis was performed using the Statistical Package for the Social Sciences (Version 18 for Windows;

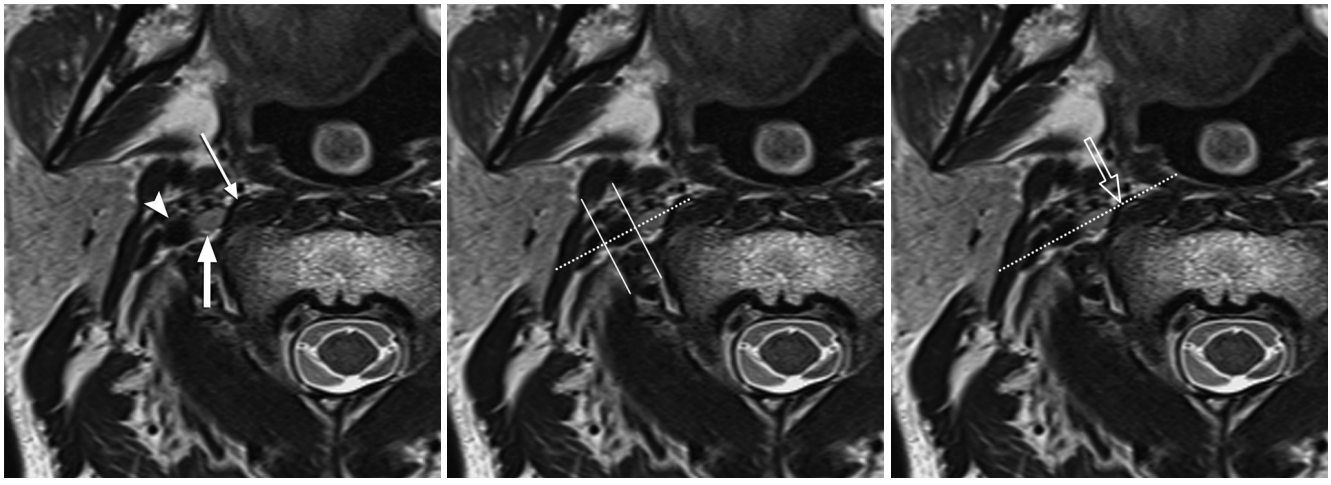

Fig. 1. Determination of relative location of superior cervical sympathetic ganglion (SCSG). Axial T2WIs at C2/3 level show defined location of SCSG (thick arrow) relative to ICA (arrowhead) and longus capitis muscle (LCM) (thin arrow). Epicenter of SCSG was criteria used to decide location. First, imaginary line (dashed lines) was drawn passing middle of ICA and SCSG. Then, two perpendicular lines (solid lines) were drawn along lateral and medial margin of ICA. Relative locations of SCSG to ICA was designated as "lateral" if it was lateral to lateral perpendicular line and "medial" if it was medial to medial perpendicular line. Between two perpendicular lines, dashed line was used to designate relative location as "anterior" or "posterior". Junction between middle and lateral one third of LCM (empty arrow) was used to designate lateral and anterior locations. ICA = internal carotid artery, T2WI = T2-weighted image

IBM, Armonk, NY, USA). Continuous variables were presented as mean ± standard deviation (SD), and categorical variables were presented as percentages. The marginal homogeneity test was used to compare the relative location of the SCSG to the ICA between the right and the left sides of the neck; the McNemar's test was used to compare the relative location of the SCSG to the LCM between the right and the left sides of the neck; and a paired *t* test was used to compare the size of the SCSG between the right and the left sides of the neck. Fisher's exact tests were used to compare the proportion of SCSGs with demonstrable intraganglionic hypointensity between definite and probable SCSGs on T2WIs, T1WIs and CE FS T1WIs, respectively. A two-sided *p* value < 0.05 was considered statistically significant. For comparison of visibility of intraganglionic hypointensity on different pulse sequences, the significance threshold for difference was set at a *p* value < 0.016 (0.05/3). Interrater and intrarater agreements for the location of probable SCSGs and the presence of intraganglionic hypointensity were investigated using an unweighted kappa value.

RESULTS

Fifteen cases were excluded during consensus reading of 106 sites of necks for the following reasons: retropharyngeal lymphadenopathy (n = 12), parapharyngeal tumor (n = 2), and surgical excision of vagal schwannoma (n = 1). Of the remaining 91 neck sites, 66 (73%) in 38 patients were identified as definite SCSGs and 25 (27%) in 15 patients were identified as probable SCSGs. The imaging characteristics of definite and probable SCSGs were homogeneous high signal intensity on T2WI, intermediate signal intensity on T1WI, and homogeneous and marked enhancement on CE FS T1WI.

Independent reading by the two radiologists revealed that 16 of the 25 probable SCSGs (64%; 18% of all SCGCs) were located anterior to the LCM and medial to the ICA; 6 (24%; 7% of all SCGCs) were located lateral to both the ICA and the LCM, and 3 (12%; 3% of all SCGCs) were located posterior to the ICA and lateral to the LCM (Fig. 2). The interrater and intrarater agreements for the relative locations of probable SCSGs were excellent (interrater agreement, κ = 0.874–0.918; intrarater agreement, κ = 0.829–0.927).

Intraganglionic hypointensity was present in 59 of the 66 definite SCGCs (89%) on CE FS T1WI, 58 of the 66 definite SCGCs (88%) on T2WI, and 21 of the 66 definite SCGCs (32%) on T1WI by reader 1; and in 60 (91%) on CE

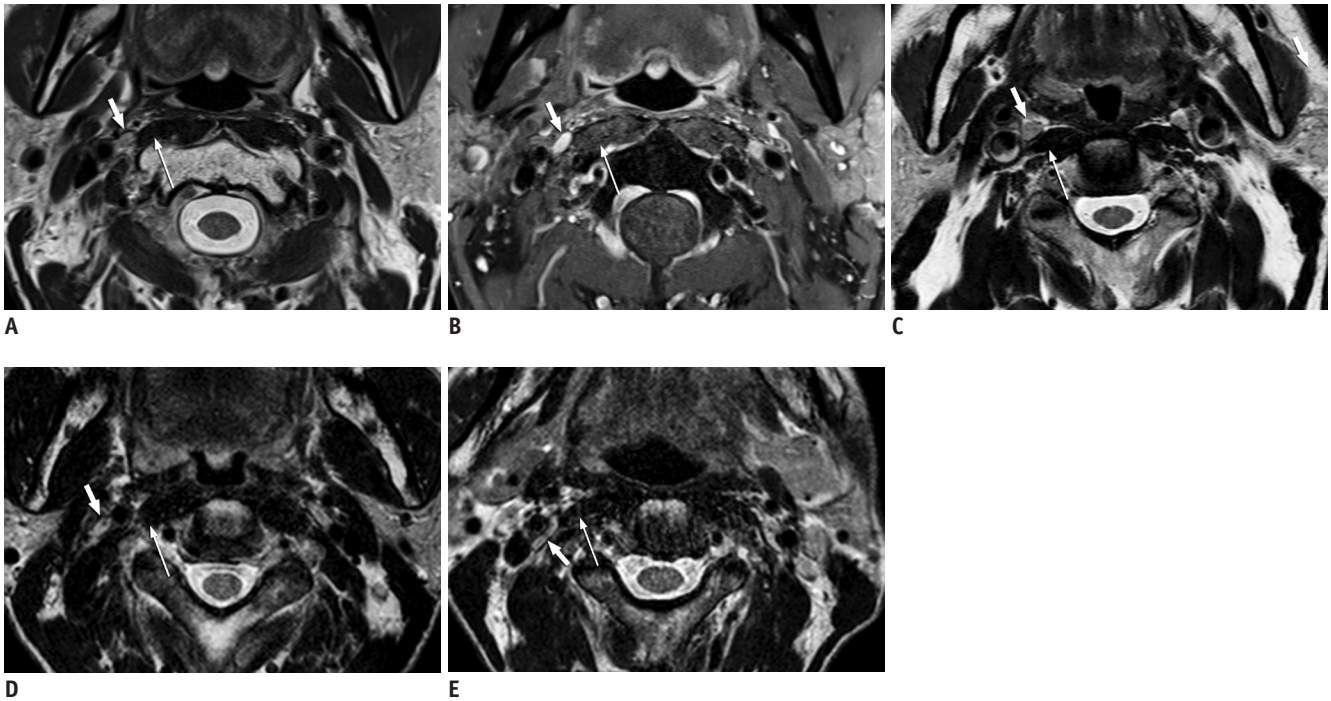

Fig. 2. Representative cases of definite SCSG and probable SCSG.
Definite SCSG (thick arrows) is evident as area of hyperintensity on axial T2WI **(A)** and homogeneous strong enhancement on contrast-enhanced fat-suppressed T1WI **(B)**, medial to ICA and lateral to LCM (thin arrows). Probable SCSGs were located anterior to LCM **(C)**, lateral to ICA **(D)**, or posterior to ICA **(E)**. ICA = internal carotid artery, LCM = longus capitis muscle, SCSG = superior cervical sympathetic ganglion, T1WI = T1-weighted image, T2WI = T2-weighted image

Korean Journal of Radiology
KJR

FS T1WI, 58 (88%) on T2WI, and 27 (41%) on T1WI by reader 2. Interrater and intrarater agreements for visibility of intraganglionic hypointensity were good-to-excellent, ranging from 0.627 to 0.779 for interrater agreement and 0.779 to 1.000 for intrarater agreement. Among probable SCSGs, intraganglionic hypointensity was present in 23 of the of 25 probable SCSGs (92%) on CE FS T1WI, 23 of the of 25 probable SCSGs (92%) on T2WI, and 8 (32%) of the of 25 probable SCSGs on T1WI by reader 1; and 22 (88%) on CE FS T1WI, 21 (84%) on T2WI, and 8 (32%) on T1WI by reader 2. Interrater and intrarater agreements for visibility of intraganglionic hypointensity were also excellent for each pulse sequence, ranging from 0.740 to 0.915 for interrater agreement and 0.839 to 1.000 for intrarater agreement. Occurrence of intraganglionic hypointensity showed no significant difference between definite and probable SCSGs for any pulse sequence (all $p > 0.05$).

The SCSGs were most commonly found at the level of the C2 vertebra (n = 61, 67%), followed by between the C2 and C3 vertebra (n = 17, 19%), and at the level of the C3 vertebra (n = 13, 14%), in order. The 91 SCSGs had maximum axial diameter (mean ± SD), 7.7 ± 1.8 mm (range, 4.8–13.2 mm), minimum axial diameter, 3.7 ± 0.9 mm (range, 2.0–6.5 mm), and longitudinal diameter, 27.9 ± 5.9 mm (range, 15.0–45.0 mm).

The relative location of the SCSG to the ICA, the relative location of the SCSG to the LCM, the size of the SCSG, or the presence of the intraganglionic hypointensity showed no significant differences between the right and the left sides of necks (all $p > 0.05$).

Susceptibility weighted imaging showed the intraganglionic hypointensity as a marked hypointense focus on the magnitude image that became hyperintense to the same degree as venous structures on the phase image, suggesting an intraganglionic vessel (Fig. 3) (15). Histologic examination of a harvested SCSG from an adult cadaver showed an SCSG with an axial diameter of 4.5 mm that was encapsulated by thick connective tissue, evenly distributed ganglionic cells, and a central vascular structure with a diameter of 0.6 mm, which was confirmed as a venule. There was no dense fibrosis or dense deposit of lipofuscin granules in the ganglion cells near the center of the SCSG (Fig. 4).

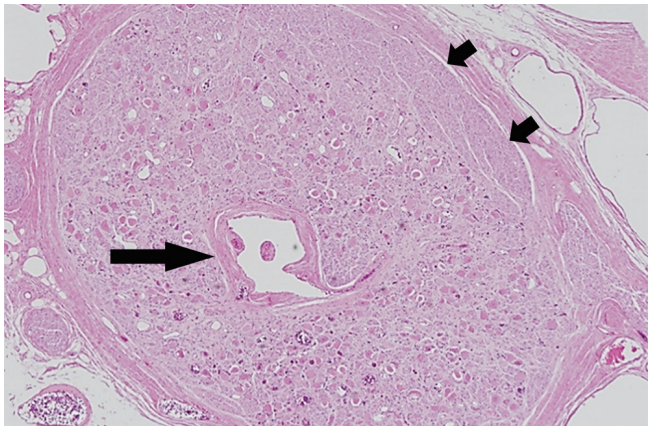

Fig. 4. Histologic examination of SCSG harvested from cadaver.
Maximum axial diameter of SCSG was 4.5 mm. Microscopic section with hematoxylin and eosin stain (x 100) shows SCSG encapsulated by thick connective tissue and nerve fibers (short arrows) arranged along periphery of SCSG. Note central vascular structure (long arrow) of 0.6 mm in diameter surrounded by numerous ganglion cell bodies, which was continuously detected on serial axial sections. SCSG = superior cervical sympathetic ganglion

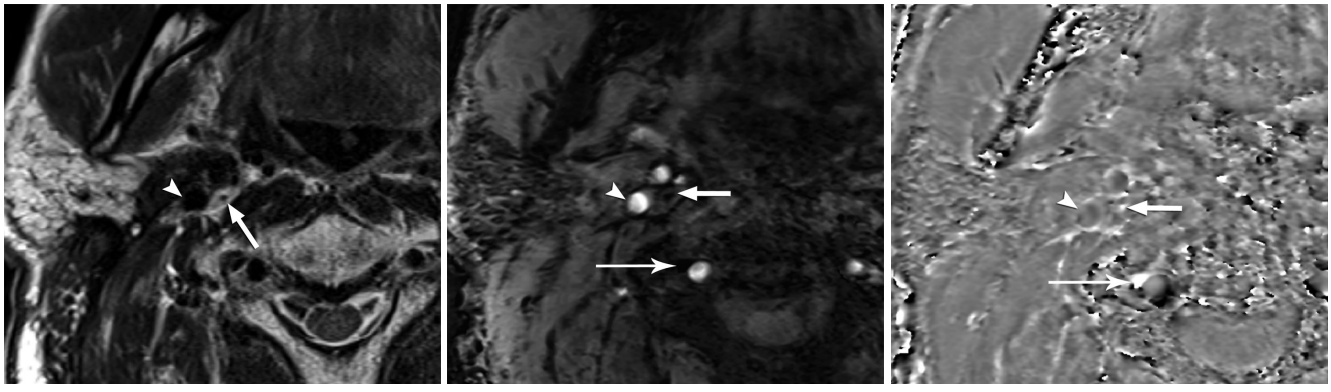

A **B** **C**

Fig. 3. SWI obtained from 59-year-old male patient.
Axial T2WI **(A)** at level of C2 vertebra demonstrate intraganglionic hypointensity (thick arrows) at center of SCSG, which is depicted with same signal intensity as paravertebral venous plexus (thin long arrows), i.e., hypointense on magnitude SWI **(B)** and hyperintense on phase SWI **(C)**. Arrowheads denote ICA. ICA = internal carotid artery, SCSG = superior cervical sympathetic ganglion, SWI = susceptibility weighted imaging, T2WI = T2-weighted image

DISCUSSION

In this study, 3T-MRI was successful in localizing 66 of 91 neck sites (73%) as definite SCSGs based on all four criteria. In the remaining 25 neck sites, probable SCSGs were anterior to the LCM and medial to the ICA (n = 16), lateral to both the ICA and the LCM (n = 6), or posterior to the ICA and lateral to the LCM (n = 3). Intraganglionic hypointensity was most conspicuous on CE FS T1WI, suggestive of potential as a distinguishing feature of SCSGs. Several cadaveric studies have focused on the normal anatomy of the SCSG with regards to surgical approach of the cervical region or cervical sympathetic block (6, 16).

Interestingly, we found that 27% of the SCSGs were not located at the position described in the literature. The probable SCSGs in this study were located more medial (anterior to the LCM) or more lateral (lateral to the ICA), and even posterior to the ICA. There could be several reasons for this variation. First, the LCM converges medially in a cranial direction (5, 6) and the cervical sympathetic trunk converges medially in a caudal direction. As the SCSG is the most superior part of the sympathetic trunk, the SCSG could be more medially located depending on the vertebral level of the SCSG. Second, the neck position for MR imaging might differ from the neck position in previous cadaveric studies (6, 14), because some of the studies were performed with hyperextension (8, 14) and rotation of the neck to the contralateral side (6) to simulate the anterior approach to the cervical spine, which might alter the relative position of SCSGs to the LCM. Third, lateral or posterior location to the ICA (10% of the probable SCSGs) has never been described in the literature and this finding could be secondary to tortuosity of the ICA (17). Because the SCSG is embedded within the deep layer of the deep cervical fascia (6), the ICA invested within the carotid sheath might change its position relative to the SCSG (18). Regardless of the causes of these anatomic variations, SCSG can vary in location relative to the ICA and may diverge from the LCM in the caudocranial direction.

Occurrence of intraganglionic hypointensity was another notable finding of this study. It was likely that the intraganglionic hypointensity was associated with a vessel or fatty connective tissue engulfed within the ganglion by traversing nerve fibers. However, microscopic examination only revealed a venule at the center with no intervening connective tissue, fibrosis, or dense deposit of lipofuscin granules in the ganglion cells. However, a final conclusion should be made with caution because the structure also appeared hypointense on CE FS T1WIs. We were unable to correlate the intraganglionic hypointensity with any histologic feature of a ganglion due to lack of reports in the literature. In addition, we have only indirect evidence in support of the structure as a venule. Therefore, further studies are required to reveal the true nature of the intraganglionic hypointensity in the near future. Despite the unclear anatomical nature of the structure, the radiological importance of the intraganglionic hypointensity is highlighted in patients with head and neck cancer with retropharyngeal lymph node metastases. Based on the occurrence of typical intraganglionic hypointensity, radiologists can confirm the paired, prevertebral, ovoid, enhanced structures at the expected location as the bilateral SCSGs rather than metastatic retropharyngeal lymphadenopathy.

The major limitation of our study is the absence of surgical confirmation of the nature of the imaging findings. Surgical confirmation was not performed, because the identified structure was strongly presumed as normal, and there are potential detrimental consequences of surgery or biopsy. Verification bias was controlled by the strict application of evidence-based criteria based on a literature review and excellent interrater and intrarater agreement. In addition, we excluded any case with confusing abnormalities in retropharyngeal, parapharyngeal, or prevertebral space or with anatomical distortion secondary to previous surgery. Another limitation is that although our additional studies suggested that the intraganglionic hypointensity might be an intraganglionic venule, this should be interpreted with caution due to the limited number of cases.

In conclusion, 3T-MRI visualized 73% of SCSGs as vertically-oriented fusiform or ovoid-shaped T2-hyperintense strongly enhanced structures located medial to the ICA and lateral to the LCM between the C2 and C4 vertebrae. The location of the remaining 27% of SCSGs was anterior to the LCM, lateral to the ICA, or posterior to the ICA. Intraganglionic hypointensity was seen in 90% of cases and could be helpful to differentiate normal SCSGs from retropharyngeal lymphadenopathy.

REFERENCES

1. Wisco JJ, Stark ME, Safir I, Rahman S. A heat map of superior cervical ganglion location relative to the common carotid artery bifurcation. *Anesth Analg* 2012;114:462-465

2. Elias M. Cervical sympathetic and stellate ganglion blocks. *Pain Physician* 2000;3:294-304
3. Tubbs RS, Salter G, Wellons JC 3rd, Oakes WJ. Blood supply of the human cervical sympathetic chain and ganglia. *Eur J Morphol* 2002;40:283-288
4. Siegenthaler A, Haug M, Eichenberger U, Suter MR, Moriggl B. Block of the superior cervical ganglion, description of a novel ultrasound-guided technique in human cadavers. *Pain Med* 2013;14:646-649
5. Som PM, Curtin HD. *Head and neck imaging*, 5th ed. St. Louis: Mosby, 2011
6. Civelek E, Karasu A, Cansever T, Hepgul K, Kiris T, Sabanci A, et al. Surgical anatomy of the cervical sympathetic trunk during anterolateral approach to cervical spine. *Eur Spine J* 2008;17:991-995
7. Kiray A, Arman C, Naderi S, Güvencer M, Korman E. Surgical anatomy of the cervical sympathetic trunk. *Clin Anat* 2005;18:179-185
8. Saylam CY, Ozgiray E, Orhan M, Cagli S, Zileli M. Neuroanatomy of cervical sympathetic trunk: a cadaveric study. *Clin Anat* 2009;22:324-330
9. Stark ME, Safir I, Wisco JJ. Probabilistic mapping of the cervical sympathetic trunk ganglia. *Auton Neurosci* 2014;181:79-84
10. Lee JH, Lee HK, Lee DH, Choi CG, Kim SJ, Suh DC. Neuroimaging strategies for three types of Horner syndrome with emphasis on anatomic location. *AJR Am J Roentgenol* 2007;188:W74-W81
11. Harris CL, Hamid B, Rosenquist RW, Schultz-Stubner SH. Ganglionic local opioid application (GLOA) for treatment of chronic headache and facial pain. *Reg Anesth Pain Med* 2006;31:460-462
12. Pozzilli P. BCG vaccine in insulin-dependent diabetes mellitus. IMDIAB Group. *Lancet* 1997;349:1520-1521
13. Yuen HW, Goh CH, Tan TY. Enlarged cervical sympathetic ganglion: an unusual parapharyngeal space tumour. *Singapore Med J* 2006;47:321-323
14. Ebraheim NA, Lu J, Yang H, Heck BE, Yeasting RA. Vulnerability of the sympathetic trunk during the anterior approach to the lower cervical spine. *Spine (Phila Pa 1976)* 2000;25:1603-1606
15. Wu Z, Mittal S, Kish K, Yu Y, Hu J, Haacke EM. Identification of calcification with MRI using susceptibility-weighted imaging: a case study. *J Magn Reson Imaging* 2009;29:177-182
16. Ding P, Tufano RP, Campbell-Malone R, Feng W, Kim SJ, German RZ. Horner syndrome after carotid sheath surgery in a pig: anatomic study of cervical sympathetic chain. *Comp Med* 2011;61:453-456
17. Wenn CM, Newman DL. Arterial tortuosity. *Australas Phys Eng Sci Med* 1990;13:67-70
18. Sacco S, Totaro R, Baldassarre M, Carolei A. Morphological variations of the internal carotid artery: prevalence, characteristics and association with cerebrovascular disease. *Int J Angiol* 2007;16:59-61